Brackish springs in coastal aquifers and the role of calcite dissolution by mixing waters

Esteban Sanz Escudé

October 19, 2007

CHAPTER 3: HYDRAULIC MODELLING OF S'ALMADRAVA BRACKISH SPRING

PhD Thesis
Department of Geotechnical Engineering and Geo-Sciences (ETCG)
Technical University of Catalonia (UPC)

Supervisors:
Dr. Jesús Carrera Ramírez
Dr. Carlos Ayora Ibáñez

Institute of Earth Sciences 'Jaume Almera', CSIC

Chapter 3

Hydraulic modelling of S'Almadrava brackish spring

Aside from constituting a curious hydraulic phenomenon yielding seawater above sea level, interest in brackish springs has grown in the last decades because of the strategic water potential of the discharges in areas with limited resources. These resources are not profitable because of salinization and therefore attempts have been made to undertake a detailed characterization of the hydrogeology and the concentration dependence on spring discharges. Most of these studies discuss the implementation of potential actions to reduce the variability and magnitude of the salinity at the spring, thus making the discharge suitable for human consumption. However, karst conduit networks can be rarely characterized at depth because of the difficulty of access. Thus, few plans to develop springs have been undertaken in practice since the application of certain actions based on partially (or even wrongly) characterized systems may lead to results that are contrary to those pursued. Numerical modeling has been successfully applied to improve different aspects of our knowledge about the functioning of brackish springs. This is considered to be a useful complementary tool to reduce the uncertainties of the conceptual models proposed for particular springs based on hydrogeological information. In Chapter 2 we described a new solver for brackish springs that reproduces the spring flow and concentration from a given freshwater flow rate in the aquifer. Numerical results obtained for a fictitious spring showed consistency with field observations from several brackish springs found in the literature.

S'Almadrava spring (Mallorca, Spain) (8 m.a.s.l.) is considered to be an outstanding example of an inland brackish spring discharging waters of increasing salinities with reducing spring flows. The spring shows a well defined pattern of salinity variation with respect to the rainfall record and develops two distinctive features hitherto undocumented, i.e., (1) high salinity (up to 60% of equivalent seawater) during the heavy rains after a long dry period and (2) a secondary salinity peak in the middle of the sharp drop in salinity after every rainfall event. This clearly reflects the complexity of the system under study. After several attempts Cardoso (1997) gave the first global explanation for spring functioning based on diverse hydrogeological and some geochemical information. Subsequently, Sanz et al. (2002 and 2003) built a preliminary numerical model to reproduce spring flow and salinity discharge based on a simple karst system. However, the hypotheses advanced to date for S'Almadrava spring did not satisfactorily account for the distinctive features of the spring. It is therefore important to review the conceptual model for the spring and to validate it with the numerical solver developed in Chapter 2.

The objectives of this study are to propose a hydraulic conceptual model for S'Almadrava brackish spring consistent with the particular hydrogeological features of the spring, and to build a numerical model to validate the conceptual model proposed and evaluate the factors controlling the functioning of the system.

3.1. Hydrogeology of S'Almadrava spring

S'Almadrava spring (8 m.a.s.l.) is located in the Pollença plain, in the northwestern area of the Island of Mallorca (Balearic Islands, eastern Mediterranean sea), a few kilometers west of the Serra Tramuntana mountains and about 2 km from the Pollença Bay (Figure 3.1). The Serra de Tramuntana mountains lie on the northern border of the Majorca Island and its structure is dominated by a system of thrusts dipping to the southeast and arranged in an imbricate system aligned NE-SW. This system was formed during the compression episodes from late Oligocene to middle Miocene, with a transport direction to NW. The complexity of the structure in the area of study has prompted a number revisions (Gelabert et al., 1992, Gelabert, 1997, López-García, 2000, among others). Regardless of the controversies, the structure in S'Almadrava hydrological unit consists of three main thrust sheets and a few minor slivers (Figure 3.1). Outcropping materials range from Upper Triassic to Quaternary in age.

Triassic materials (Keuper and Rhaetian) appear as a low permeable rhythmic bedding of clays, marls, evaporites and volcanic rocks changing to dolomites and marls towards the top, with a variable thickness (up to 350 m) due to tectonic phenomena. They represent the main decollement levels of the thrust system, thus playing a key hydrological role in limiting the Liassic aquifers (Figure 3.1). In the spring area, two Liassic aquifers are identified, separated by a variable thickness of Dogger-Malm marls. Liassic materials are composed of fractured

dolomites, calcites and carbonated breccias with a variable thickness of 250 to 300 m. These materials are highly permeable due to fracturation. The top of the confined aquifer has been found at approximately at -320 m.a.s.l. in deep cores drilled near the spring mouth, and extends below -570 m.a.s.l. (López-García, 2000) (Figure 3.1). In addition to fracturation, the Liassic materials are extensively affected by karst development (Ginés and Ginés, 2002, Encinas, 1997). Encinas (1994) described and mapped over 500 karstic cavities only in the western Serra de Tramuntana, some of them extending several hundreds of meters horizontally and tens of meters vertically. In the plain of Pollença, where the spring discharges, only few karst cavities have been described but this situation is attributed to the fact that they may be collapsed or partially refilled by the Quaternary materials, thus making the determination of the location difficult (J.A. Encinas, personal communication). The karstification is well developed also at depth as demonstrated in cores from deep drillings in the vicinity of the spring (C. González, personal communication). The Miocene materials are turbidites series of marls with some sandstone intercalations, presenting low permeabilities. These materials crop out tilted but their continuity at depth is not known in detail. Quaternary clays and conglomerates appear covering small depressions in the surface.

S'Almadrava spring discharges directly into a stream on Liassic carbonates but near the discontinuity contact with overlying post-tectonic Miocene turbiditic materials (Fornós and Gelabert, 1995). It represents the most important discharge point of the S'Almadrava hydrological unit. The precise definition of the hydrological boundaries of this unit is not easy owing to the complex tectonic structure but it is accepted that its geometry and boundaries fit roughly with those of the Axartell thrust sheet (Gelabert, 1997). Groundwater flow and aquifer response is mainly controlled by the high hydraulic conductivity of the Liassic karstified system and the geological structure (Van Meir et al., 2006). Groundwater flow lines are parallel to the thrust direction (NE-SW with direction to NE) and most of them converge on S'Almadrava spring.

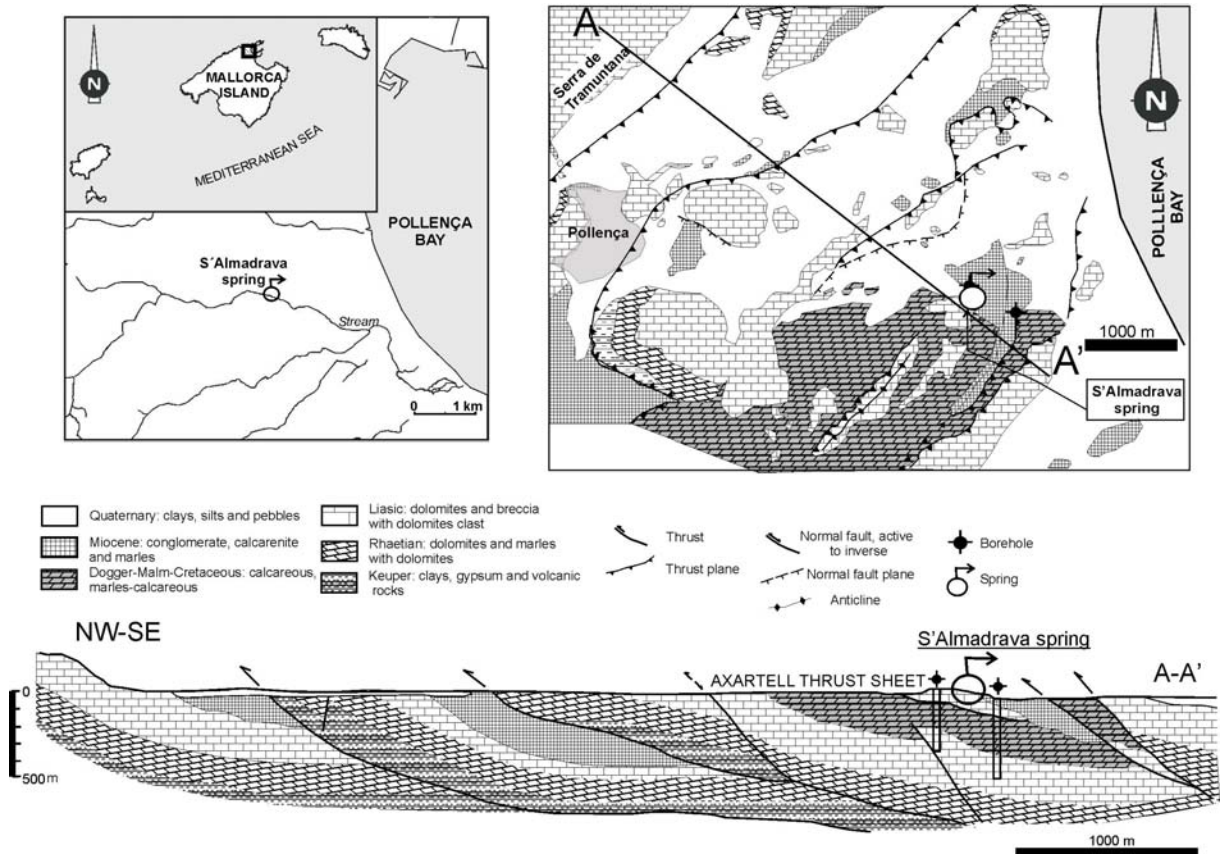

Figure 3.1: Location map of S'Almadrava spring in Mallorca (top left), geological map of the area around the spring (top right) and a geological cross section perpendicular to the main structure in the proximity of the spring mouth (bottom), after López-García (2000).

The recharge area of the spring extends over some 50 km^2 on the Serra de Tramuntana and part of the Pollença plain. The climate is Mediterranean with annual average temperatures of 15 ºC (monthly averages ranging from 8 to 26 ºC) and about 900 mm/y of precipitation. Precipitation is irregularly distributed, concentrating in sharp rainfall events roughly once every 4-8 weeks from autumn to spring. Summer is usually a long rainless season (Figure 3.2). The spring discharge presents short pulses and fast responses to rainfall events, with a spectral correlation analysis consistent with that of a well-developed karst system (Cardoso, 1997). In fact, the maximum flow discharge is reached 24 to 48 hours after a rainfall event is produced, although the flow discharge increases from just 8 hours after (Figure 3.2).

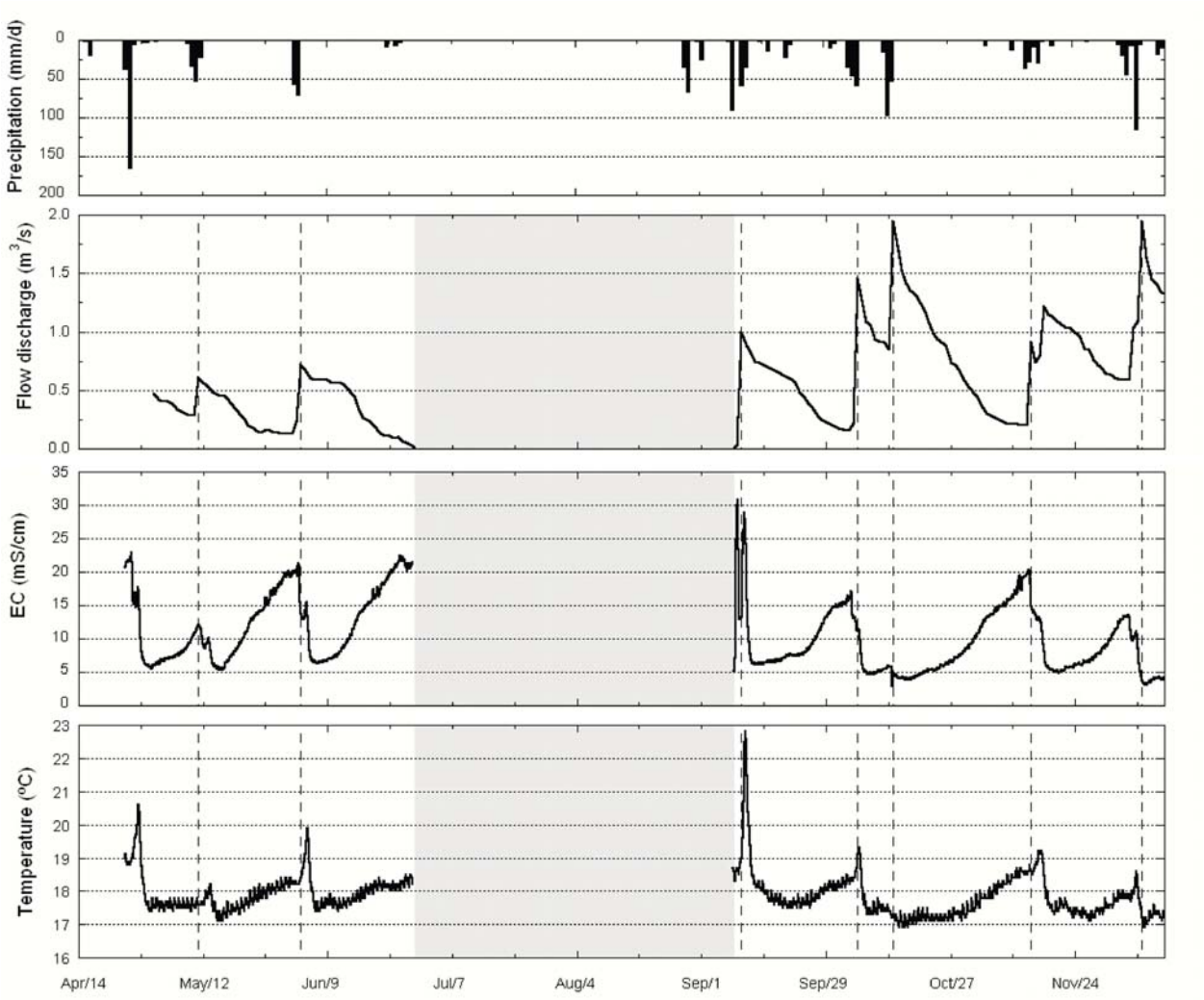

Figure 3.2: Field measurements of rainfall at the recharge area, spring flow discharge, electrical conductivity (EC) and temperature of S'Almadrava spring inj 1996. Grey area shows the period when the spring is dry. Dashed lines mark the moments of maximum flow discharge for every run-off event.

A considerable amount of historical data is available for S'Almadrava spring. Early government reports (MOPU-DGOH, 1973; SHB, 1987) initiated the collection of hydrological data in the spring, suggesting the connection of its particular behavior with the highly karstified carbonate aquifer. Barón and González (1978) performed a systematic control of chloride concentration at the spring and studied the relationship between the salinity and discharge of the spring. The spring discharge and rainfall in the recharge area (daily), and the electric conductivity (EC) and temperature of the discharge (hourly) have been monitored irregularly in the last decade. Flow discharge was measured at a gauging station in the stream near the spring mouth, the contribution of the stream to the measured flow rate being negligible, except for high peak discharges (since the stream regime is also strongly influenced by the rainfall events). Figure 3.2 displays the hydrological data obtained in 1996, which is considered to be representative of the spring behaviour. Yearly spring discharge equals 12.3 Mm^3/y on average

(ranging from 6 to 24 Mm^3/y). EC fluctuates in a well-defined range of 5 to 20 mS/cm, although values of up to 30 mS/cm (60% equivalent seawater) were measured during spring reactivations after a long dry period. Temporal variation of EC depends strongly on discharge, clearly showing an increase in salinity with decreasing spring discharge (Figure 3.3). These variations reproduce a sequence of cycles that commence whenever a new rainfall event is produced (Figure 3.2). This constitutes a characteristic pattern that has been maintained over the years. Thus, salinity increases slightly at the start of significant rainfall events before declining sharply. Subsequently, it increases again gradually as the discharge rate comes to and end. When a new rainfall event recommences a new cycle is initiated (Figure 3.2). However, when no rainfall events are produced for more than 6-8 weeks, the spring discharge decreases dramatically and the spring eventually dries up. This situation usually occurs during the long rainless summer season (Figure 3.2).

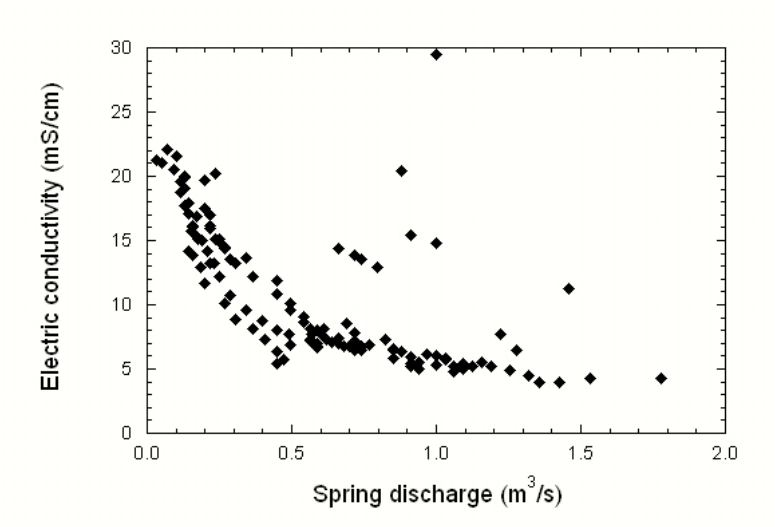

Figure 3.3: Relationship of electrical conductivity and spring discharge observations for S'Almadrava spring in 1996. Field measurements correspond to daily observations.

In addition to the cyclic behaviour described, S'Almadrava spring displays two distinctive features. One arises during the first rainfall event after a long dry period in which the spring remains dry. Under these conditions, salinity undergoes a sharp increase together with the discharge flow, reaching the highest salinity values recorded before rapidly decreasing (Figure 3.2). On closer inspection,, this high salinity peak is in reality two peaks. This situation does not result from any variation in spring discharge, but from the structure of the spring. Figure 3.2 shows how, after this unusual increase in salinity, the spring initiates the cyclic pattern described above with the gradual increase in EC up to about 20 mS/cm.

The second distinctive feature is the secondary salinity peak, which appears in the middle of the sharp salinity drop after a rainfall event (Figure 3.2). Note that this peak is observed in every

spring cycle and must therefore result from a well developed feature of the karst network feeding the spring. The secondary peak last only for a couple of days before salinity continues to decrease.

The temperature of S'Almadrava spring displays a temporal variation similar to that of salinity, with an increase in temperature for decreasing discharge flows. Temperatures are in a range of 17 to 20ºC with maximum values (up to 23ºC) recorded for the first rainfall events after a long dry period (Figure 3.2). Compared with EC records, the temperature shows a unique temperature peak of several degrees during the spring reactivation after a long rainless period and no secondary temperature peaks have been reported. However, an increase in temperature is reported with every increase in spring discharge. Minor temperature oscillations observed in Figure 3.2 reproduce day/night temperature cycles.

Finally, although it may be assumed that seawater contributes to spring salinity, Cardoso (1997) suggested that the dissolution of Keuper evaporites at the base of the carbonated main aquifer may contribute to salinity, especially when the spring dries up and the residence time in the aquifer increases. However, the $\delta^{34}S$ and $\delta^{18}O$ values of the sulfate dissolved in S'Almadrava spring samples show an excellent agreement with a conceptual model of pure mixing of seawater intruding into the freshwater aquifer. The influence of other potential sources of salinity, such as Keuper evaporites or fertilizers, has been estimated to be very limited at any stage of the hydrological cycle of the spring (Appendix A).

3.2. Hydraulic conceptual model for S'Almadrava spring

Any conceptual model proposed to explain the functioning of brackish springs must include the existence of a well developed deep karst system and identify the dominant mechanism of salinization, i.e., mainly the way in which seawater intrudes into the aquifer and mixes with freshwater (see Chapter 2). Our proposed conceptual model for S'Almadrava spring assumes that groundwater circulates mainly through a network of interconnected conduits and seawater contamination is produced at a deep conduit branching. Seawater intrusion into the conduit branching would be produced through a karst conduit connecting directly with the sea (Figure 3.4). Although diffusive seawater contamination from the porous matrix could also play a role in S'Almadrava spring, this is expected to be minor since groundwater flow in the deep limestone aquifer near the coast has been reported to be mainly driven by few well developed conduits (Van Meir et al., 2006). Note that the dashed lines in Figure 3.4 represent a conduit of undefined shape open directly to the sea. In fact, the depth of the sea outlets does not affect the spring response to brackish springs that do not behave as submarine springs at any stage (Chapter 2). In the case of S'Almadrava, no submarine outlets have been reported in the Pollença bay so this simplification is reasonable. Moreover, the ratios of equivalent freshwater-

seawater flow rates measured in the spring are consistent with these observations since they show that the spring operates in a range of flow discharges far below the minimum fresh flow rate required to form a submarine spring (Chapter 2) (Figure 3.5).

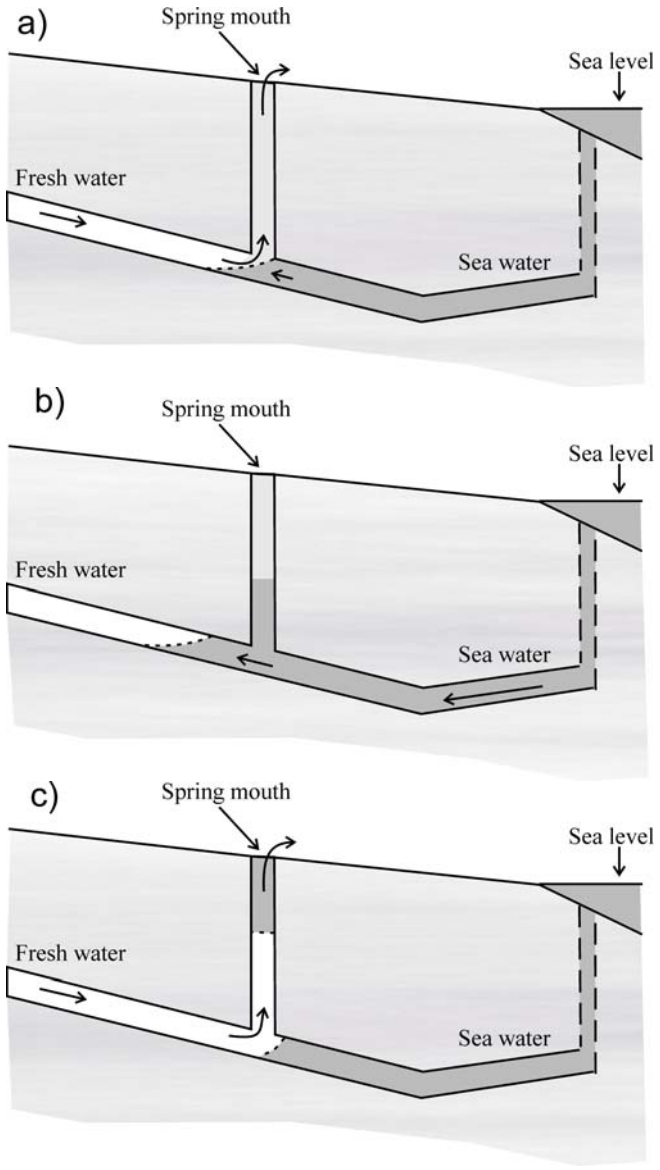

Figure 3.4: Scheme of the hydraulic conceptual model for S'Almadrava spring, which considers salinization at a conduit branching from a conduit connected to the sea, and a single conduit connecting the branching point to the spring mouth. Three situations are shown: a) mixing of waters is produced at the conduit branching during a spring cycle and the spring discharges brackish water; b) long dry period during which seawater intrudes into the conduit branching and the freshwater conduit; and c) a new rainfall event is produced and the freshwater drags the high salinity water towards the spring mouth. Softer grey areas represent the (very low permeability) matrix. Water salinity in the conduits increases from white to dark grey.

In such a conduit network environment, groundwater flow follows the hydraulic laws for pipes, that can be simplified into a mass and energy balance at the conduit branching (Chapter

2). When the interface between freshwater and seawater is placed at the conduit branching, this point becomes contaminated by mixed water of variable density. This density is a function of the energy at the conduit branching (Figure 3.4a). This would explain the dependence of salinity with the spring discharge observed for S'Almadrava spring (Figure 3.3). When freshwater flow rate decreases, the mixing ratio at the conduit branching (and in the vertical conduit) increases although there is a decrease in the seawater flow rate. This reduction is controlled by the limiting weight of the water column connected to the spring mouth (Figure 3.5). This is due to the fact that the energy necessary to move the water upwards increases with the weight of the water column in the conduit connected to the spring mouth. Low freshwater flow rates in the aquifer allow more seawater to mix because of the increase in the energy gradient between the conduit branching and the open sea, and vice versa (Chapter 2).

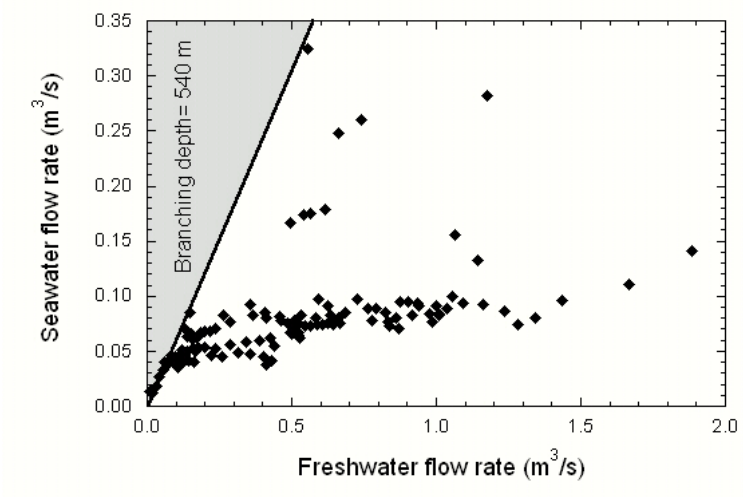

Figure 3.5: Relationship of equivalent freshwater and seawater of the S'Almadrava spring discharge in 1996. Field measurements correspond to daily observations. The grey area marks freshwater-seawater ratios out of the estimated potential range for a conduit branching at -540 m.a.s.l.

Finally, when the freshwater flow rate approaches zero, the energy necessary to push up a column of water is too high and the spring could eventually dry up as in summer (Figure 3.2). During this season, water needs in the area are covered from pumping wells on the Liassic aquifer. This pumping may also affect the equilibrium at the conduit branching, allowing seawater to intrude further into the freshwater conduit in the aquifer (Figure 3.4b). When a new rainfall event is produced, the freshwater flow rate arriving at the conduit branching is large enough to drag this high salinity water towards the spring mouth and to move the mixing interface seawards (Figure 3.4c). The result is an important spring discharge of unusually high salinity, as recorded at S'Almadrava (Figure 3.2). To account for the phenomenon of high spring

discharges with high salinity it is not necessary to assume the existence of conduit narrowings and high flow velocities, which would be difficult to find in nature (Chapter 2).

In order to define the depth at which the conduit branching is located, we propose in Chapter 2 an approximation based on field observations of concentration and flow discharge (eq 2.18). When the freshwater flow rate at the conduit branching decreases approaching zero, the average density at the vertical conduit connected to the spring mouth reaches its highest value before the spring dries up. At this point, the weight of the water column (the maximum sustainable) equals that of the seawater from the conduit branching to the sea level. Therefore, one could deduce the depth of the conduit branching from the elevation of the spring mouth and an approximation of the average density in the vertical conduit (Chapter 2, eq (2.18)). Taking the density of the spring discharge before it dries up as a reasonable approximation of the average density, the minimum depth of the conduit branching in S'Almadrava spring is calculated to be -540 m.a.s.l. Note that the relation between the depth of the conduit branching and the maximum potential mixed water density also provides the minimum ratio of equivalent freshwater-seawater discharging in the spring. The grey area in Figure 3.5 illustrates the freshwater-seawater ratios out of the estimated potential range, showing an excellent agreement with the field data of the spring. This minimum depth for the conduit branching to be located at is also consistent with the depth of the deeper Liassic carbonate aquifer near the spring.

Temperature variations at the spring mouth may be interpreted as indicators of differences in temperature of freshwater and seawater in the aquifer before they mix together, or of the residence times in the system. Given the estimated depth of the conduit branching, the geothermal gradient is sufficient to account for these observations. Yet, to explain the fact that temperature is maximum at the secondary peak, it must be complemented by either two depths of circulation of the mixing waters or two residence times of those waters in the aquifer.

With this conceptual model S'Almadrava spring would be classified as "spring contaminated owing to the greater density of seawater in karst aquifer showing anisotropic permeability" in the classification proposed by Breznik (1973), and as "systems with well-developed karstification below sea level and open to the sea (type 2) in the classification proposed by Fleury et al. (2007a).

3.3. Single conduit numerical simulation

3.3.1. Model settings

The hydraulics of the conceptual model proposed are governed by mass and either momentum or energy conservation. In this study we use the iterative algorithm programmed in

FORTRAN, called TURBOCODE, which solves the equations governing variable density pipe flow derived in Chapter 2. It allows the simulation of groundwater flow through a conduit branching, where a conduit with freshwater joins one with seawater connected to the sea. The mixed water flows upwards to the spring mouth in a turbulent mode through a well developed conduit. The procedure of TURBOCODE consists of calculating the flow and transport independently for every conduit in the system and determining, through an iterative process, the seawater flow rate that accomplishes energy equilibrium at the conduit branching for each time step. Transport is solved by means of a particle tracking method that gives the spatial distribution of concentrations at every time step (Chapter 2). Note that the solver was not designed to predict the spring flow rate from rainfall input data, but rather to understand the mechanisms causing the salinity variations of S'Almadrava spring.

Table 3.1: List of parameter values used in single conduit and dual permeability simulations for S'Almadrava spring. The parameter values represent the optimal values after calibration to reproduce field measurements in 1996 (Figure 3.2).

	Single conduit model	**Dual permeability model**
L_s	4000.0 m	4000.0 m
A_s	0.23 m^2	0.21 m^2
n_s	2.0x10^{-2}	2.0x10^{-2}
z_B	-540 m.a.s.l.	-540 m.a.s.l.
n_{mT}	1.5x10^{-2}	1.5x10^{-2}
A_{mT}	1.0 m^2	1.0 m^2
k_{mD}	x	1.0x10^{-6} m^2
A_{mD}	x	100.0 m^2

Simulations were performed in transient conditions with a time-dependent freshwater input flow obtained from field measurements in 1996. The parameter values used in the simulations are listed in Table 3.. Symbols L_s, A_s and n_s stand for the length, section and manning number of the seawater conduit, respectively; A_{mT} and n_{mT} for the section and manning number of the mixed water conduit; and z_B for the depth of the conduit branching. These parameters were obtained after calibration and are consistent with geological and hydrological

features of S'Almadrava spring. The freshwater and seawater mixing solutions were defined as having a salt mass fraction of 6.74×10^{-4} and 3.57×10^{-2}, respectively.

3.3.2. Results and discussion

The model was calibrated for a 200 day time interval in 1996 (Figure 3.2), including two series of spring cycles separated by a long dry summer season. The results of the model calibration are compared with the field data observations in Figure 3.6. Our model reproduces satisfactorily the sharp salinity decrease at the beginning of a new discharge event and the gradual increase in salinity with the spring discharge decrease between two consecutive rainfall events. These series of cycles are the most characteristic pattern of S'Almadrava spring. The simulation also reproduces the maximum concentration in the spring, before it dries up during the summer, and the high salinity values recorded with the first rainfall event after the summer. The comparison of simulation results and observations in terms of Q_s vs Q_f, and c_m vs Q_m (base value, left column, Figure 3.7) also indicates the good performance of the numerical simulation as well as that of the conceptual model. Therefore we can conclude that the model reproduces the main patterns of the spring response in both the wet and dry seasons and is able to explain the physics of the spring functioning.

However, the simulation does not reproduce satisfactorily the spring response at particular stages of the period simulated (e.g., in the first spring cycle, Figure 3.6). In fact, Figure 3.7 shows some spreading of the field observations that would impede the fitting of all the measurements into one curve. On the other hand, it is clear that the simplicity of the single conduit conceptual model prevents us from reproducing the secondary salinity peaks occurring when a new rainfall event takes place. A more complex hydraulic conceptual model should be considered to reproduce these simulations.

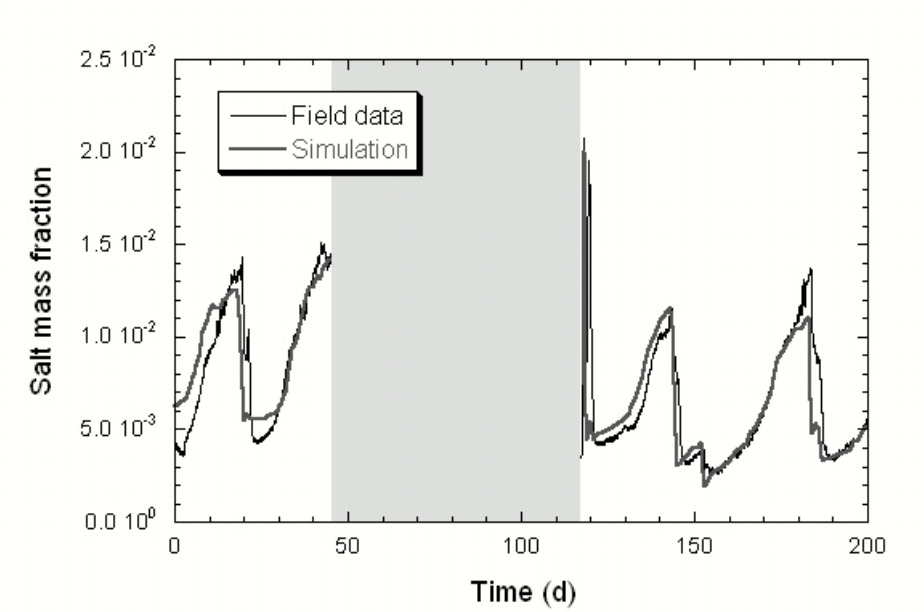

Figure 3.6: Comparison of salt mass fraction variation in field observations (black thin line) and in the single conduit simulation results (grey bold line) for S'Almadrava spring concentrations during a period in 1996.

Additional simulations were designed to check the sensitivity of the model with respect to the resistance to flow in the seawater conduit (as n_s) and the vertical conduit (as n_{mT}), and to the depth of the conduit branching (z_B). These three parameters ultimately control the results for this conceptual model (Chapter 2). The sensitivity analysis improved the model calibration and provided some insights into the functioning of S'Almadrava spring. The analysis was performed by perturbing the parameters in ±20% with respect to the base values resulting from the calibration discussed earlier (Table 3.1). Figure 3.7 shows the results of the freshwater-seawater ratio and the relationship of spring concentration and discharge. The usefulness of these relationships is that they can be compared directly with field observations.

The results of the sensitivity analysis are consistent with earlier discussions in Chapter 2. The solution when the freshwater flow approaches zero is only influenced by the depth of the conduit branching (Figure 3.7a and b). That is, the maximum density (or salt mass fraction) of the spring discharge only depends on the depth of the conduit branching. This observation supports our earlier discussion on the ability to approximate the depth of the conduit branching from the elevation of the spring mouth and the spring salinity before it dries up. Thus, the best fit is achieved for depth of -540 m.a.s.l. (base value, Figure 3.7a and b). A deeper conduit branching has higher energy and allows denser water to reach the spring mouth.

The proportion of seawater entering the conduit branching decreases with the resistance to flow in both the seawater and the mixed water conduits. I.e., the energy losses in the system (Figure 3.7c and e) impede the intrusion of more seawater into the system. However, their effect

is different for each conduit. A higher value of n_s increases the energy loss in the seawater conduit and a lower seawater flow rate is able to intrude into the conduit branching for a particular freshwater flow rate (Figure 3.7c and d). This effect attenuates when the freshwater flow rate approaches zero (i.e., very low spring discharges) because the energy loss is a quadratic function of the flow and the solution becomes controlled by the weight of the water column connected to the spring (Figure 3.7c and d). The salt mass fraction of the spring discharge also reduces its dependency with n_s for high spring discharges (approx. over 1.5 m^3/s) because the solution for this range of spring discharges turns out to be dependent on the depth of the conduit branching and the energy losses in the vertical conduit. This attenuation is expected to continue if higher spring discharges are measured at S'Almadrava. On the other hand, the solution is clearly only sensitive to n_{mT} for high spring discharges. It should be noted that because the variation of the seawater flow rate is masked by the high freshwater flow rate, the 20% variation of n_{mT} has little effect on the variation in the salinity of the spring discharge (Figure 3.7f). Therefore, in the case of S'Almadrava spring, the resistance to flow in the mixed water conduit was due to the group of parameters with the highest uncertainty during the calibration. By contrast, this simulation is not sensitive to n_{mT} for relatively low freshwater flow rates because in these situations the solution merely depends on the balance between the weight of the mixed water column and that of seawater to the sea level.

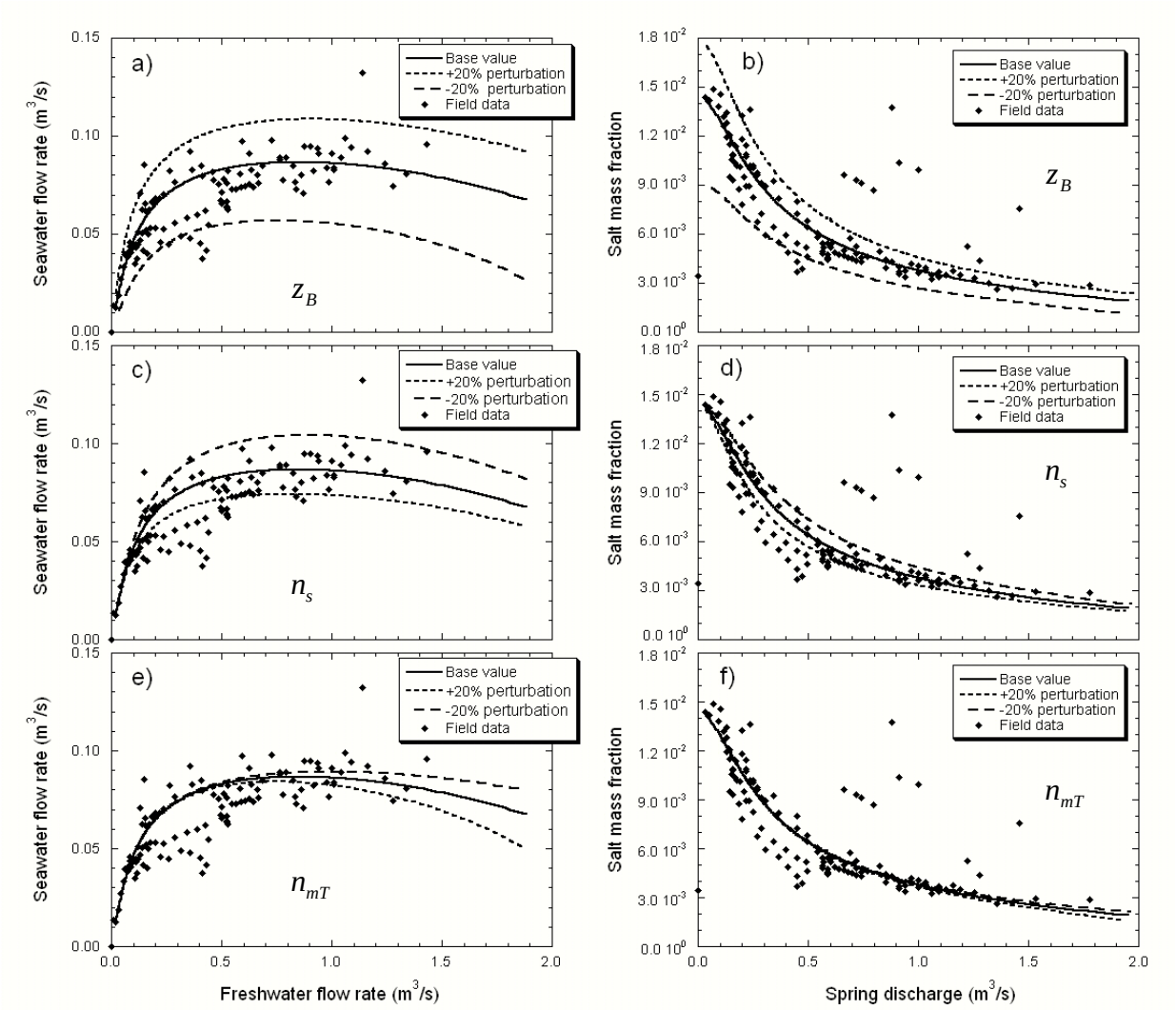

Figure 3.7: Sensitivity analysis for the single conduit simulation for S'Almadrava spring with respect to a and b) the depth of the conduit branching (z_B); c) and d) the resistance to flow in the seawater conduit (as n_s); and e) and f) the resistance to flow in the vertical conduit (as n_{mT}). This figure shows the freshwater-seawater ratio curve (left column) at the conduit branching, and the relationship of spring discharge and concentration (right column). Simulation results (lines) are compared with field observations (black diamonds).

3.4. Dual permeability numerical simulation

3.4.1. Model settings

A more complex hydraulic conceptual model is proposed for S'Almadrava spring in order to explain the secondary salinity peaks observed when a new rainfall event is produced. Although different scenarios may be proposed at this stage, we propose that the secondary peaks result from a dual permeability system for the mixed water flowing from the conduit branching to the spring mouth. Thus, the mixed water flowing upwards divides into two pathways: a fast turbulent

flow through a well developed karst conduit, and a slow flow through a network of smaller fractures (matrix) surrounding the conduit. The latter flow passes through a considerably wider porous area that is governed by the Darcy's law. The higher residence time in the fractured matrix with respect to that of the open conduit would result in a delay in the arrival time of the high salinity mixed water to the spring mouth, thus generating a secondary salinity peak. Figure 3.8 illustrates a scheme of the dual permeability conceptual model proposed. S'Almadrava spring's outlet is located not only at a main point of discharge but also at several minor outlets, all of them discharging into the same stream. This observation lends support to the hypothesis, that there is a non negligible flow through the matrix surrounding the vertical karst conduit. The proximity of the spring outlet to the discontinuity contact of the limestone made up of Miocece turbiditic materials at depth (Figure 3.1) also favours the existence of a partially porous flow in such a contact.

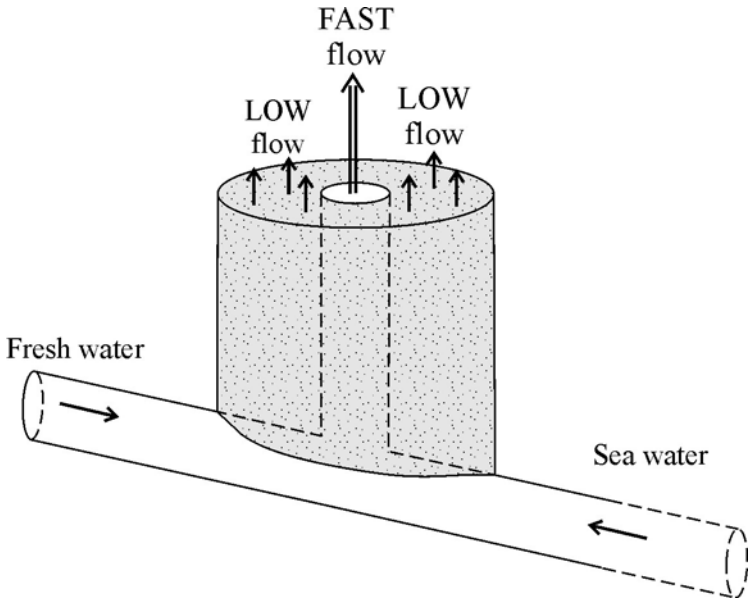

Figure 3.8: Scheme of the dual permeability hydraulic conceptual model for S'Almadrava spring which considers contamination of seawater at the conduit branching from a conduit connected directly to the sea and a dual permeability medium linked to the spring mouth. Mixed water flow from the conduit branching to the spring mouth is divided into a fast component through a well developed karst conduit and a slow flow through a network of fractures and fissures.

In order to solve the dual permeability case, a modification was programmed in TURBOCODE consisting of a double iteration algorithm that achieves the optimal distribution of the mixed water flowing upwards independently in the two media. It should be pointed out that the solver does not reproduce any potential mass transfer between the open conduit and the porous matrix. Following the explanations in Chapter 2, the flow is governed by mass and either

momentum or energy conservation, while the balance in the conduit branching is maintained in terms of fluid mass, solute mass and energy. That is

$$Q_{mT}\rho_{mT} + Q_{mD}\rho_{mD} = Q_f\rho_f + Q_s\rho_s \quad (3.1)$$

$$Q_{mT}\rho_{mT}c_{mT} + Q_{mD}\rho_{mD}c_{mD} = Q_f\rho_f c_f + Q_s\rho_s c_s \quad (3.2)$$

and

$$H_{BmT} = H_{BmD} = H_{Bs} \quad (3.3)$$

where the subindex f stands for freshwater, s for seawater, m for mixed water, B for conduit branching, and T and D for the conduits governed by a turbulent and a Darcy flow, respectively (for an explanation of other symbols, see Chapter 2). H_{BmT}, and H_{BmD}, the energies of the conduits at the conduit branching, result from eq (2.6):

$$H_{BmT} = P_{BmT} + \rho_m \frac{v_{mT}^2}{2} = \overline{\rho_{mT}} g\left(L_{mT} + \frac{L_{mT} n_{mT}^2 Q_{mT}^2}{A_{mT}^2 R_{HmT}^{4/3}}\right) + \rho_{mT-mouth} g \frac{v_m^2}{2} \quad (3.4)$$

$$H_{BmD} = P_{BmD} = L_{mD}\left(\frac{Q_{mD}\mu}{A_{mD}k_{mD}} + \overline{\rho} g\right) \quad (3.5)$$

where $L_{mT} = L_{mD}$ but $A_{mT} \neq A_{mD}$. The energy of the conduit connected to the sea at the conduit branching, H_{Bs}, is expressed by eq (2.16).

Simulations for the dual permeability model were performed also in transient conditions, with the same time-dependent freshwater input flow used for the single conduit simulations, obtained from field measurements in 1996. The parameter values obtained after calibration are listed in Table 3.1. Note that when applicable, the same parameter value was used in both the single conduit and the dual permeability simulations, except for a minor adjustment of the section in the seawater conduit, A_s.

3.4.2. Results and discussion

In a dual permeability scheme, the proportion of the mixed water flowing through the conduit branching that moves upwards in the karst conduit or the fractured matrix depends on two factors: the energy loss and the weight of the water column (i.e., the average density) in every medium. For simplification, let us consider that both vertical media are filled with the mixed water at the conduit branching. This implies that the two media have the same water column weight and that only the effect of the energy loss will be observed. The solution is converted into a steady-flow simulation with near zero residence time in the conduits. The results obtained under these conditions for the parameter values on Table 3.1 are shown in Figure 3.9 (lines). It

may be observed that the flow rate through the open conduit is faster than through the fractured matrix for slow spring discharges. This is attributed to the relatively higher energy loss of the fractured matrix. However, as the spring discharge increases, the energy loss increases more rapidly in the open conduit (resistance changes quadratically with flow rate, compared with the linear dependency for Darcy's flow). Thus, the proportion of groundwater flowing through the karst conduit decreases with the spring discharge with the result that the flow rate through the matrix is higher (spring discharges over 1.6 m^3/s in Figure 3.9). It should be noted that, although the flow rate through the fractured matrix is higher than that of the open conduit, the residence time in the matrix continues to be much lower than in the open conduit. This is so because the porous area in the matrix is a 100 times greater than the conduit section (Table 3.1). Therefore, the fast flux in the system always occurs in the karst conduit.

The difference in the water column weight in the conduit and matrix can only be observed with simulations in transient conditions. As discussed above, during a spring depletion period after a rainfall event, the density of the water mixing at the conduit branching increases with the decrease in the spring discharge. Therefore, the density of the water entering the two vertical media also increases with time, giving rise to a variable density profile in the water column. But because of the different residence times, these density profiles and the average density in the water column will be different in the two media. Given that the velocity in the open conduit is much higher than that of the fractured matrix, the average density in the open conduit is also higher, and the difference in the average densities increases with the depletion time. For high spring discharges and high water velocities in the conduits the formation of density profiles is negligible and the solution approximates that of the steady-flow (Figure 3.9). As the story of the spring proceeds, the creation of the density profiles becomes appreciable and the solution progressively differs in behaviour from that of the steady-flow (from 1.2 to 0.8 m^3/s, aprox. in Figure 3.9). Owing to the fact that the water column weight of the conduit is greater than that of the matrix, the energy efficiency of the system reduces the flow rate through the conduit with respect to the steady-flow solution. If the difference between the water column weights continues to increase, the proportion of the flow rates in the two media is inverted and the flow rate through the matrix exceeds that of the karst conduit (spring discharges below 0.6 m^3/s approx. in Figure 3.9). Thus, although for very low spring discharges most of the flux passes through the matrix, the difference in the average densities of the water columns is never compensated given that the residence time of the water in the karst conduit continues to be smaller.

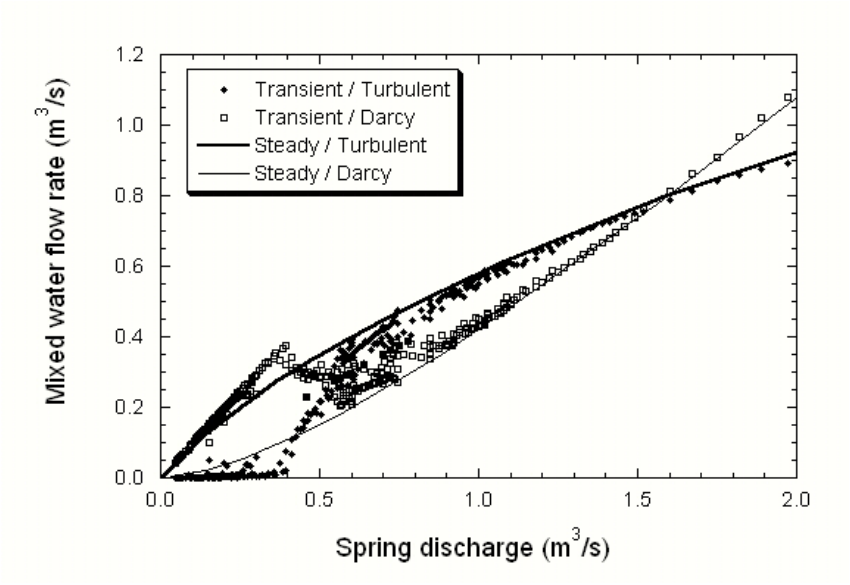

Figure 3.9: Distribution of flow rates of mixed water in the karst conduit and in the network of fractures in steady flow conditions (average density of the water column equals that of the conduit branching) (lines) and transient simulations for S'Almadrava spring in 1996 (symbols). The parameter values used in the simulations are in Table 3.

The combination of the formation of different density profiles together with the differences in flow rates and residence times in the two media accounts for the formation of secondary salinity peaks for S'Almadrava spring. Figure 3.10 shows the performance of dual permeability model for the secondary salinity peaks observed in S'Almadrava spring during the two first rainfall events after the summer of 1996 (see calibration parameter in Table 3.1). The model reproduces satisfactorily the field observations for both the double high salinity peaks after the long dry summer season (day 117), and the minor secondary peak in the middle of the concentration drop after every rainfall event (day 145). The results confirm that the dual permeability concept model explains and reproduces the distinctive features of the salinity variation at S'Almadrava. The minor disagreements in the reproduction of the field observations can be attributed to the fact that no mass transfer between the open conduit and network of fractures was reproduced despite being possible in nature.

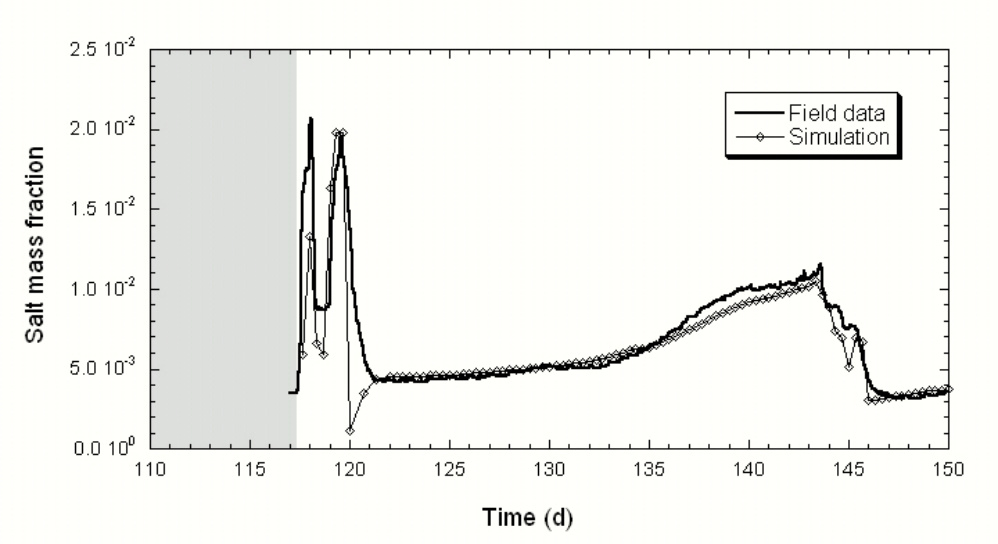

Figure 3.10: Comparison of salt mass fraction variation in field observations (bold line) and in the dual permeability simulation results (thin line with empty diamonds) for S'Almadrava spring, during the two first rainfall events after the summer of 1996. Grey area shows the period when the spring is dry. Time scale agrees with that of Figure 3.6.

In the dual permeability model, the formation of the secondary salinity peaks depends on only two parameters: the section (A_{BmD}) and the intrinsic permeability (k_{BmD})of the fractured matrix. These parameters control the residence time (i.e., the differences in density profiles, and thus the arrival delay) and the flow rate (i.e., the distribution of the total water volume through the conduit branching in the two media) in the matrix. We performed a sensitivity analysis with respect to these two parameters and the results are shown in Figure 3.11. Note that the results shown in Figure 3.11 are plotted in two separated time intervals for a better representation. Both parameters increase the proportion of flow rate through the fractured matrix, but their effect on the spring response is different. This is due to two factors: (1) the fact that perturbing A_{BmD} does not significantly change the residence time in this medium, and (2) the delay of the arrival of the high density waters flowing through the matrix at the spring mouth is practically the same. Further, the formation of secondary salinity peak should show little sensitivity to A_{BmD}. However, the extremely high dynamic behavior of the system causes the small variations in the proportions of flow rates in the conduits to yield apparently wrong results (Figure 3.11a and b). In other words, the afore-mentioned delay in the arrival of high salinity waters from the matrix will not be reflected in the spring salinity if its water volume is not big enough to avoid dilution when mixning with the freshwater from the karst conduit. The results of the model show a strong dependence on the porous area of the fractured matrix for the spring depletion period between consecutive rainfall events (Figure 3.11a and b). Increasing the porous area of the matrix

reduces the concentration of the spring discharge given that it increases the proportion of the less dense water from the matrix with respect to the denser water from the karst conduit.

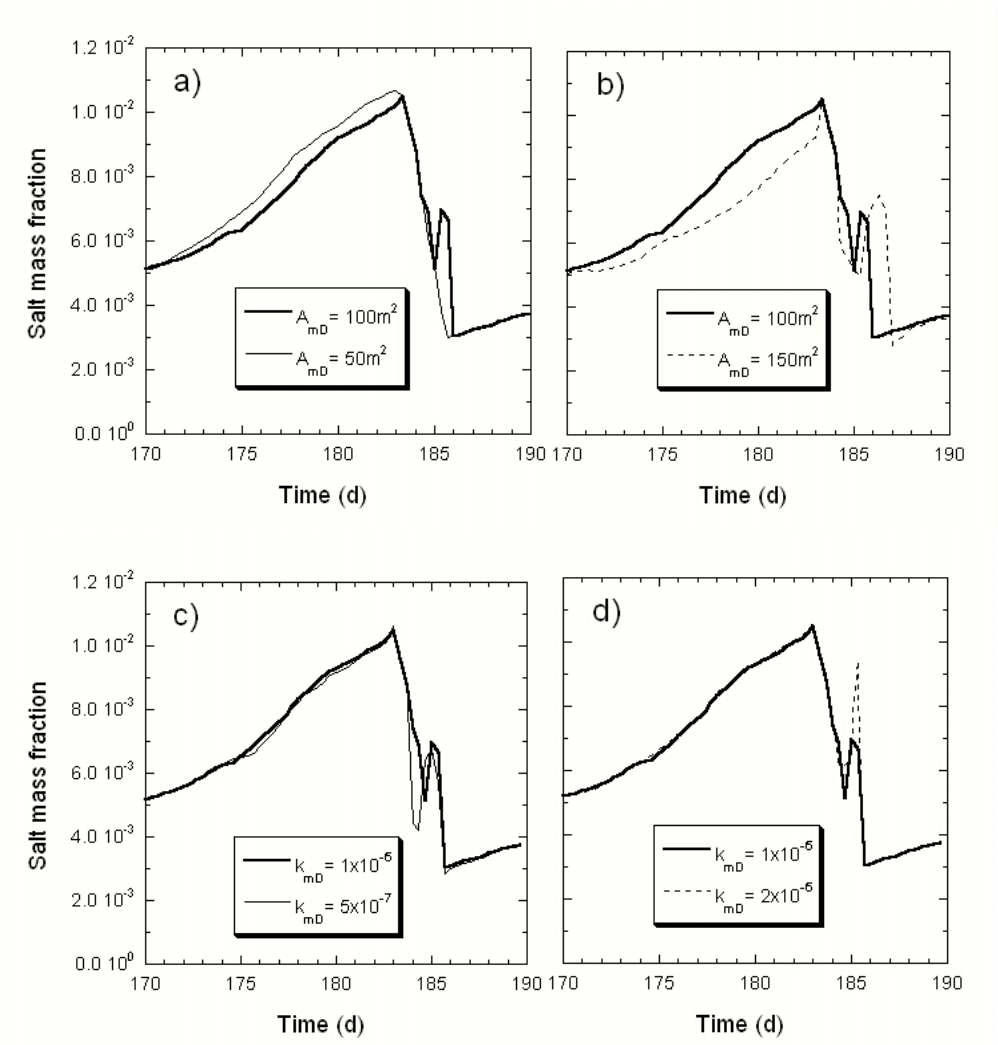

Figure 3.11: Sensitivity analysis of the variation of salt mass fraction of S'Almadrava spring for the dual permeability model, with respect to: a) and b) the section to flow of the fractured matrix; and c) and d) the intrinsic permeability of the fractured matrix. Bold line represents the base simulation in all the cases. The time period reproduced corresponds to the second rainfall event after the summer of 1996. Time scale agrees with that of Figure 3.6 and Figure 3.10.

On the other hand, raising the k_{BmD} will increase both the flow rate and velocity of the water in the matrix. Lower permeabilities will produce sharper drops of salinity with the rainfall events and more delayed secondary salinity peaks (Figure 3.11c). The secondary salinity peak appears to be well defined after the spring discharged low salinity water. Higher permeabilities produce the secondary peak very close in time to the salinity drop and on occasions may be difficult to distinguish (Figure 3.11d). Note that permeability has little influence on the increase

of salinity for the period between consecutive rainfall events. This is so because the variation of flow rate through the fractured matrix is proportional to the variation of flow velocity.

3.4.3. Conceptual model discussion

Simulations performed in this study show that the proposed hydraulic conceptual models of different complexity are able to reproduce the response of S'Almadrava spring at different levels of detail, and the results suggest the validation of these conceptual models from a hydraulic point of view. Both the single conduit and the dual permeability conceptual models demand the existence of a well developed karst system at depth, assuming the existence of a conduit branching located at -540 m.a.s.l. (or deeper), and a connection with the open sea through a karst conduit of a relatively small section (Table 3.1). In order to account for the formation of a karst network at such depth in the S'Almadrava area, we have to consider a combination of different factors. First of all, the limestone aquifer appears highly affected by tectonic constraints during its formation, including thrust sheets and associated tiny fractures. Fracturing controls the groundwater flow in the limestone aquifers and therefore concentrates the dissolution potential of the groundwater in a few major fractures. Dissolution has enlarged the sections of these fractures creating a well developed network of karst conduits, which has been extensively reported in the area (Ginés and Ginés, 2002, Encinas, 1997). These karst conduits could be formed by freshwaters above sea level during geological periods of sea level fall. Subsequently, the elevation of the sea level either by tectonic subsidence or sea level rise could promote the flooding of the existing conduits and the formation of new ones. A stacked network of interconnected conduits would then be created. Gràcia et al. (2001) quantified the sea level drop during the Riss and Würm glaciations to a depth of -130 m down with respect to current sea level. Thus, the sea level variations during glacial periods may not be sufficient to explain the estimated depth of the conduit branching of S'Almadrava spring and a larger-scale event of sea level fall should be taken into account. This could be the case of the Messinian salinity crisis at the end of the Miocene, which produced a sea level fall of about 1500 m over the entire duration of the crisis (Ryan, 1976, and Clauzon, 1982, in Fleury, 2007a).

In addition to sea level variations and tectonics, the role of non-linearities of carbonate species in a mixing solution is likely to contribute to the enlargement of the karst networks at any depth, but especially at the conduit branching. It is well known that mixing of solutions of different chemical compositions and dissolved carbonate species, which are both saturated with respect to calcite can result in undersaturated conditions if the original groundwaters have different CO_2 partial pressures, pH, temperatures, etc (Wigley and Plummer, 1976). In fact, Ginés (2000) highlighted the role of mixing fresh and seawater in the coastal phreatic zone of Mallorca Island, especially removal of rock wall and collapse debris by enhanced dissolution. Rezaei et al. (2005) also quantified the importance of mixing processes in the porosity

development in coastal areas affected by seawater intrusion. The role that mixing solutions may have in porosity development in carbonate coastal aquifers is extensively discussed in Chapters 5 and 6.

Despite the limited information on karst network distribution at depth for S'Almadrava, we propose that the freshwater flow in the S'Almadrava unit concentrates in karst conduits parallel to the thrust sheet direction, increasing in depth to the northeast. This freshwater would mix with the seawater at conduit branching located in the deeper liassic aquifer. The mixed water would eventually flow up through karst conduits and tiny fractures (the equivalent fractured matrix) associated with the discontinuity contact with Miocene materials. However, as pointed out by Cardoso (1997) it is not possible to confirm the ascent of the mixed water though the Miocene-Liassic contact because the distribution of these materials at depth is still not well understood.

3.5. Conclusions

A revised hydraulic conceptual model was proposed for S'Almadrava spring. This model assumes the existence of a conduit branching at a minimum depth of -540 m.a.s.l. (based on field observations) and connection with sea through a karst conduit of a small section. The mixed water flows up very quickly mainly through a karst open conduit, resulting in a fast response of the system to the rainfall events. A numerical model was built to reproduce this single conduit conceptual model for S'Almadrava spring with satisfactory results. The model reproduces the main patterns of the salinity variation of the spring in both dry and wet seasons, in 1996. Thus, the model was able to explain the physics of the system controlling the S'Almadrava spring response. The sensitivity analysis of the simulation is performed with respect to the energy loss in the seawater and mixed water conduits, and with respect to the depth of the conduit branching. The solution displays a high sensitivity to the depth of the conduit branching for the whole range of spring discharges. The flow resistance of the seawater and mixed water conduits affects only medium and high spring discharges, respectively.

In addition to this single conduit model, a more complex conceptual one was also proposed to account for the occurrence of the distinctive features of S'Almadrava spring: double high salinity peaks after a long dry season and secondary salinity peak immediately after a new rainfall event. These salinity variations point out the high complexity of the karst systems. Because of the limited information on the karst network distribution at depth, different conceptual models could be proposed to explain these secondary peaks. We propose the existence of a dual permeability model, where the mixed water flowing from the conduit branching to the spring mouth divides into two flows: a fast flow through a karst conduit (akin to the single conduit conceptual model), and a slow flow through a fractured matrix (equivalent to a porous medium). Simulation results for this complex model show a very good agreement with

the field observations. They account for the occurrence of the double high salinity peak after the dry summer season, and the secondary peak in the middle of the salinity drop after a rainfall event. The solution for this case is extremely dependent on the difference in the water column weight in the two media and therefore requires the use of transient simulations. The formation and extent of the secondary salinity peak largely depends on the porous area and the hydraulic permeability of the matrix.